CO_2 hydrogenation over guanidine-treated Fe-Co catalysts

Edgar Ma

Jericho High School

Abstract: Climate change and fossil fuel depletion are becoming increasingly severe issues in the 21st century. CO_2 hydrogenation, a gas-phase CO_2 catalytic conversion method, can be used to mitigate the effects of climate change and renewably produce value-added chemicals such as light olefins. Fe-Co bimetallic carbides have shown good potential for CO_2 hydrogenation. However, carbide synthesis remains a challenge. Guanidine has shown promise in catalysis and could be used to induce carburization in Fe-Co catalysts. Fe_2-Co_6-CeO_2 and Fe_2-Co_6-CeO_2-G were synthesized and preliminarily tested on a flow-bed reactor and gas chromatograph (GC). In-situ diffuse reflectance infrared Fourier transform spectroscopy (DRIFTS) and residual gas analysis (RGA) were used to analyze the surface chemistry and determine reaction intermediates of Fe_2-Co_6-CeO_2-G. GC testing showed improved activity on Fe_2-Co_6-CeO_2-G compared to Fe_2-Co_6-CeO_2, with higher CO_2 conversion and light olefin production, suggesting guanidine induced carburization. DRIFTS and RGA indicate the occurrence of reverse water-gas shift (RWGS) and Fischer-Tropsch synthesis (FTS). Carbonate and formate were detected by DRIFTS and showed correlation with RWGS activity, suggesting the simultaneous occurrence of the carbonate and formate pathways over Fe_2-Co_6-CeO_2-G. Future studies should focus utilize X-ray diffraction (XRD) and X-ray photoelectron (XPS) spectroscopy to elucidate the phase of Fe_2-Co_6-CeO_2-G, and determine whether carburization had occurred and whether it contributed to the increased CO_2 hydrogenation activity. XPS can also be used to further study the reaction mechanism and confirm whether the formate and carbonate pathways were occurring. Overall, guanidine treatment on Fe-Co catalysts is promising for CO_2 hydrogenation.

Introduction

Climate change is becoming an increasingly severe issue in the 21st century. The impacts of climate change are estimated to cost hundreds of billions of dollars in the U.S. economy in the following decades [1]. The greenhouse effect is the primary cause of climate change, with carbon dioxide being the biggest contributor to the greenhouse effect, comprising 82% of greenhouse emissions in 2017 [2]. In addition to climate change, fossil fuel depletion is another major issue. The depletion of fossil fuels is expected to have major implications for the global economy [3].

Carbon dioxide conversion is a method that can be used to mitigate the greenhouse effect by recycling waste CO_2. It can also provide a renewable source of value-added chemicals used as fuels and in industry, such as light olefins, which would otherwise be derived from fossil fuels [4]. CO_2 hydrogenation, a gas-phase carbon dioxide conversion method, utilizes the reverse water-gas shift reaction (RWGS) in conjunction with the Fischer-Tropsch synthesis (FTS) to produce value-added chemicals from CO_2 [5]. The two most commonly accepted mechanisms for RWGS are the formate dissociation and redox pathways. In the formate pathway, CO_2 is hydrogenated to formate, and the carbonyl bond is cleaved [6]. The redox pathway generally occurs on Cu catalysts. Cu^0 is oxidized to Cu^+ by CO_2, resulting in CO formation, while H_2 reduces Cu^+ to Cu^0 and forms water [7]. However, a less commonly accepted pathway is the carbonate pathway. In the carbonate pathway, hydroxyls react to form H_2O and O^{-2}. O^{-2} reacts with CO_2 to form carbonates, which then react with H_2 to form CO and hydroxyls [8].

Transition metal carbides have often been cited as promising catalysts for CO_2 hydrogenation, due to high CO_2 adsorption and ability to dissociate hydrogen and carbonyl bonds [6], [9]. Iron carbides in particular have shown favorable performance for CO_2

hydrogenation [10], [11]. In addition, bimetallic Fe-Co carbide catalysts have shown increased CO_2 and CO conversion for FT synthesis, indicating their potential for CO_2 hydrogenation [12]. There are currently obstacles in synthesizing effective iron carbides for CO_2 hydrogenation. Current methods for synthesizing iron carbides include sol-gel methods, solid state reaction methods, and wet chemical synthesis methods [11].

Guanidine is an organic compound shown to have catalytic properties. Guanidine-based materials have been used to catalyze various biological and biochemical reactions. One example is in biodiesel production [13], [14]. Guanidine could act as a carbon source, making it a potential candidate to induce carburization in Fe-Co catalysts. In addition, the guanidine's role as a reducing agent may increase catalyst activity [15]. The goals of this study were to determine the effects of guanidine treatment on CO_2 hydrogenation activity over a bimetallic Fe-Co catalyst over CeO_2 support and determine possible reaction intermediates and pathways of the CO_2 hydrogenation mechanism over the guanidine treated catalyst.

Methods and materials

Materials

Iron powder, cobalt powder, and citric acid to synthesize the polymeric complexes. CeO_2 was used as support for both catalysts. Guanidine was used to treat the Fe-Co catalyst. All chemicals were obtained from Sigma Aldrich, St. Louis, MO.

Polymeric complex synthesis

Iron polymeric complex (IPC) was synthesized using 28 g iron powder, and 96.5 g citric acid. These were mixed into deionized water to form the solution.. Afterward, solid IPC was obtained from the solution by evaporating out excess solvent. Solid cobalt polymeric complex (CPC) was obtained in a similar manner, using 29 g cobalt powder and 96.5 g citric acid.

Catalyst synthesis

To synthesize the Fe_2-Co_6-CeO_2 catalyst, 0.0627 g IPC and 0.01910 g CPC were physically mixed. The metallic complex mixture was then physically mixed into 1.4546 g of CeO_2 support. The Fe_2-Co_6-CeO_2-G catalyst was prepared in a similar process; 0.0627 g IPC, 0.01910 CPC, and 0.606 g guanidine were physically mixed, and 1.4546 CeO2 support was physically mixed in afterward. Fe_2-Co_6-CeO_2 and Fe_2-Co_6-CeO_2-G were calcined under air and N_2, respectively, for 5 hours. Both catalysts were compressed, hand milled, and separated by particle size into three groups: 177 μm-250 μm, 250 μm-420 μm, and powder.

Catalyst performance testing

Preliminary catalyst testing was done over a flow-bed reactor. Product gasses were quantified using on-line gas chromatography (GC). The catalysts were tested at 275°C, 300°C, and 325°C under reaction gas.

Evaluation of activity and surface chemistry

In-situ diffuse reflectance infrared Fourier transform spectroscopy (DRIFTS) and residual gas analysis (RGA) were used to evaluate catalyst activity and determine reaction intermediates

on Fe_2-Co_6-CeO_2-G. For DRIFTS measurements, a BRUKER XSA and a BRUKER VERTEX 70 were used for reflectance and transmittance, respectively. 250 μm-420 μm size catalyst particles were loaded into the testing chamber. The catalysts were reduced under H_2 for one hour at 300°C. Afterward, the temperature was dropped to 250°C. Reaction gas consisting of 8 mL/min He, 8 mL/min CO_2 and 24 mL/min H_2 was flowed through the DRIFTS unit. Temperature was increased by 25°C approximately every 30 minutes. One DRIFTS scan was taken per minute. The RGA measured a fraction of output gas from the in-situ DRIFTS reaction.

Results and discussion

Catalyst performance

GC measurements were taken to analyze products formed over the catalysts and evaluate catalyst performance. The Fe_2-Co_6-CeO_2-G catalyst shows increased performance compared to the Fe_2-Co_6-CeO_2 catalyst. This indicates that the guanidine treatment enhanced CO_2 hydrogenation activity over the Fe-Co catalysts.

Table 1: Fe_2-Co_6-CeO_2 GC performance. The Fe_2-Co_6-CeO_2 product yields were quantified by integrating the GC data. The Fe_2-Co_6-CeO_2 catalyst shows no activity across all temperatures, indicating that the non-guanidine treated catalysts could not engage in CO_2 hydrogenation.

Temperature	CO_2 Conversion (%)	Selectivity (%)				C_2-C_3 Yield (%)
		C_2-C_3	CH_4	C_2H_6	$C3H_8$	
275°C	0	0	0	0	0	0
300°C	0	0	0	0	0	0
350°C	0	0	0	0	0	0

Table 2: Fe_2-Co_6-CeO_2-G GC performance. The Fe_2-Co_6-CeO_2 product yields were quantified by integrating the GC data. The Fe_2-Co_6-CeO_2-G catalyst shows improved CO_2 hydrogenation activity compared to Fe_2-Co_6-CeO_2.

Temperature	CO_2 Conversion (%)	Selectivity (%)				C_2-C_3 Yield (%)
		C_2-C_3	CH_4	C_2H_6	$C3H_8$	
275°C	11.07	2.400	94.40	0.805	1.705	0.264
300°C	12.05	5.770	91.52	0.928	1.598	0.695
350°C	11.19	8.720	66.96	13.27	11.06	0.976

The Fe_2-Co_6-CeO_2 does not show activity (**Table 1**), with no CO_2 conversion occurring at any temperatures. However, good CO_2 conversion was seen on the Fe_2-Co_6-CeO_2-G catalyst (**Table 2**). Peak CO_2 conversion occurred at 300°C at 12.05%. In addition, the Fe_2-Co_6-CeO_2-G catalyst shows substantial production of light olefins, with the peak selectivity occurring at 325°C at 8.720%. These results suggest that carburization may have occurred on the Fe_2-Co_6-CeO_2-G catalyst, which led to light olefin production and overall improved performance compared to Fe_2-Co_6-CeO_2. It should be noted that during GC testing, the methane and CO peaks could not be separated. As a result, part of the methane selectivity is attributed to CO formation.

Catalyst activity

DRIFTS and RGA were used to determine the activity of the catalyst in terms of RWGS and FTS through adsorbed species and output gas. CO and H_2O concentrations increase stepwise with temperature for Fe_2-Co_6-CeO_2-G (**Fig. 1**).

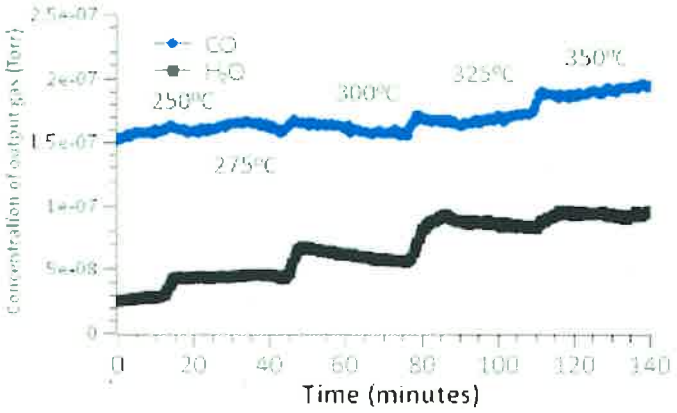

Figure 1. **RGA of H_2O and CO output concentrations for Fe_2-Co_6-CeO_2-G**. Stepwise increases with temperature indicate the occurrence of RWGS.

Because RWGS is endothermic and favored at high temperatures, this stepwise increase suggests the occurrence of RWGS. This data indicates that RWGS is promoted by the Fe_2-Co_6-CeO_2-G. RWGS is the first step in CO_2 hydrogenation, indicating that the guanidine treatment did enhance CO_2 hydrogenation activity. The promotion of RWGS allows for the overall CO_2 hydrogenation process to be more efficient, as increased CO production allows for the increased production of hydrocarbons.

The DRIFTS data show peaks occurring at 886.09 cm^{-1} and 818.16 cm^{-1} (**Fig. 2a**), which can be indexed to gas-phase CO [16]. Due to software limitations, the CO peaks are shown as inverse peaks.

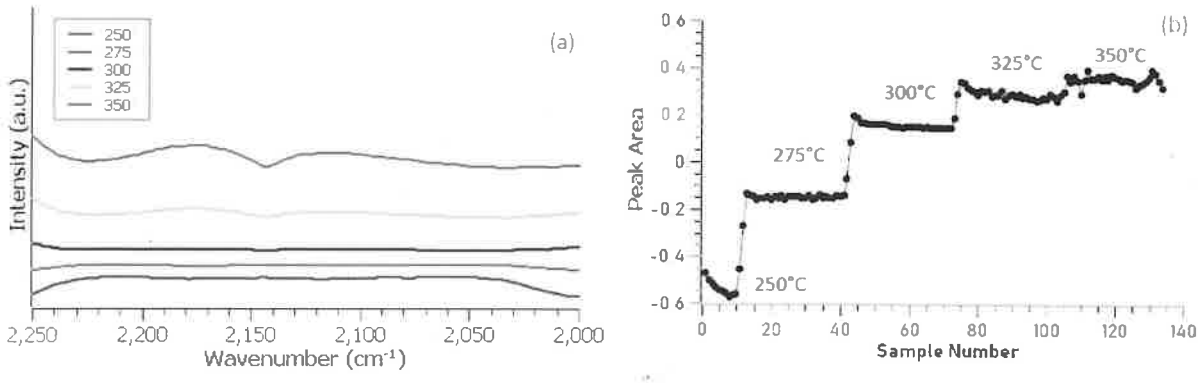

Figure 2: **CO formation over Fe_2-Co_6-CeO_2-G.** (a) Representative spectra in CO region. (b) Integrated peak areas between 886.09 cm^{-1} and 818.86 cm^{-1}. Representative spectra selected near middle of total set of scans for each temperature. Stepwise increases in integrated peak area suggest RWGS.

The integrated peak areas show stepwise increases in CO with temperature (**Fig. 2b**). This is consistent with the RGA data, and further supports the occurrence of RWGS on both catalysts.

Peaks between 3033.68 cm^{-1} and 2991.65 cm^{-1} can also be seen (**Fig. 3a**). These peaks can be indexed to methane [17]. As with the CO data, the methane peak at 250°C shows as an inverse peak. Though methane is generally an unwanted product, these results indicate the occurrence of FTS, which further suggests that CO_2 hydrogenation had occurred over Fe_2-Co_6-CeO_2-G.

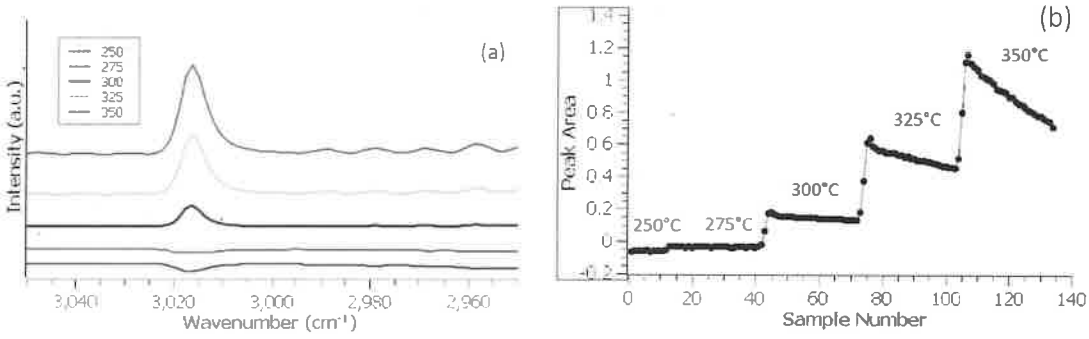

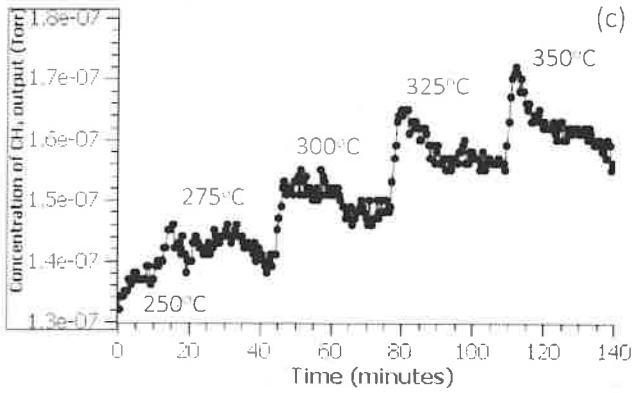

Figure 3: **Methane formation over Fe_2-Co_6-CeO_2-G.** (a) Representative DRIFTS spectra in methane region. (b) Integrated peak areas between 3033.68 cm^{-1} and 2991.65 cm^{-1}. (c) RGA output concentrations of methane. Formation of methane suggests occurrence of FTS.

The integrated peak areas and methane concentrations in the RGA data both show stepwise increases in methane with temperature (**Fig. 3b and 3c**). Because of RWGS activity increasing with temperature, it follows that methane formation would increase due to increased quantities of CO participating in FTS.

Reaction intermediates

In-situ DRIFTS was also used to identify adsorbed species and determine possible intermediates of the reaction. Fe_2-Co_6-CeO_2-G shows peaks between 2921.2 cm^{-1} and 2765.7cm^{-1}, with inverse peaks occurring at 250°C (**Fig 4a**). These peaks can be indexed to formate [18], [19].

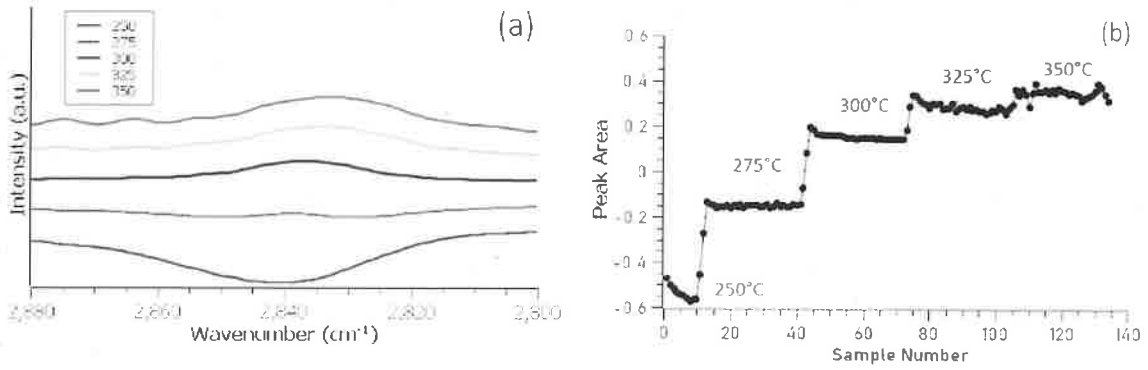

Figure 4: **Formate formation over Fe2-Co6-CeO2 surface.** Representative DRIFTS spectra at each temperature for (a) Fe2-Co6-CeO2 (b) Fe2-Co6-CeO2-G. Integrated peak areas between 2921.2 cm^{-1} and 2765.7cm^{-1}, corresponding to formate. Formate increases stepwise with temperature.

The formation of formate occurs in a stepwise manner, increasing with temperature **(Fig. 4a and 4b).** This correlates with the RWGS reaction, indicating that formate is formed as an intermediate of RWGS. These results indicate that the RWGS reaction occurs along the formate decomposition pathway.

Fe_2-Co_6-CeO_2 and Fe_2-Co_6-CeO_2 also show peaks between 886.09 cm-1 and 818.86 cm-1 **(Fig. 5a)**, which can be indexed to carbonate [20]. An inverse peak occurs at 250°C.

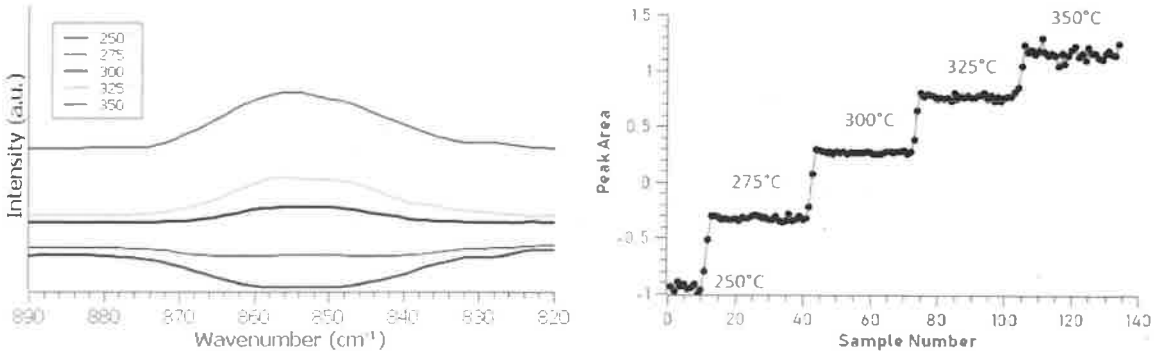

Figure 5: **Carbonate formation over Fe2-Co6-CeO2 surface.** Representative DRIFTS spectra at each temperature (a) Fe2-Co6-CeO2 (b) Fe2-Co6-CeO2-G. Integrated peak areas between 886.09 cm^{-1} and 818.86 cm^{-1}. Stepwise increases can be seen with temperature.

As with formate, the integrated peak areas of carbonate appears to show stepwise increases with temperature (**Fig 5b**), indicating that it is also possibly an intermediate of the pathway. The presence of carbonate indicates that the carbonate pathway is also occurring in this reaction. Because formate and carbonate species were both observed on the catalyst, it is possible that the carbonate pathway and formate pathway occur simultaneously in the RWGS reaction.

Conclusion

The Fe_2-Co_6-CeO_2-G catalyst showed increased CO_2 hydrogenation compared to Fe_2-Co_6-CeO_2, which suggests that carburization was induced by the guanidine treatment. GC testing of Fe_2-Co_6-CeO_2-G showed good selectivities for olefin production and increased CO_2 conversion. In-situ DRIFTS and RGA suggest that RWGS and FTS occurred over Fe_2-Co_6-CeO_2-G. Carbonate and formate species were formed on the catalyst, and appeared to be correlated to RWGS, indicating their presence as RWGS intermediates. These suggest that the RWGS reaction occurs along both the formate and carbonate pathways.

In the future, catalyst characterization methods such as X-ray diffraction (XRD) and X-ray photoelectron spectroscopy (XPS) should be used to understand the crystallographic and electronic properties of the catalyst. These could help elucidate how the guanidine treatment had affected the catalyst chemically and structurally, and definitively determine whether the guanidine treatment induced carburization. Aside from carburization, previous studies have

shown that bimetallic interactions and metal-support interactions could also affect catalytic performance [21], [22], [23], [24], [25]. Understanding the chemical and structural properties will help ascertain whether carbide formation led to increased CO_2 hydrogenation activity, or whether one or a combination of these other factors were the cause. In addition, XPS can be used to study the RWGS reaction mechanism in more detail and confirm whether the carbonate and formate pathways were occurring over Fe_2-Co_6-CeO_2-G.

Overall, these results show that guanidine treatment is a promising method for increasing CO_2 hydrogenation activity over Fe-Co catalysts. Future adoption of guanidine-treated Fe-Co catalysts could improve CO_2 hydrogenation efficiencies and contribute to a net reduction of CO_2 emissions. [26], [27], [28].

References

[1] J. Martinich and A. Crimmins, "Climate damages and adaptation potential across diverse sectors of the United States," *Nature Climate Change*, vol. 9, no. 5, pp. 397–404, Aug. 2019.

[2] "Overview of Greenhouse Gases," *EPA*, 11-Apr-2019. [Online]. Available: https://www.epa.gov/ghgemissions/overview-greenhouse-gases. [Accessed: 30-Sep-2019].

[3] M. Höök and X. Tang, "Depletion of fossil fuels and anthropogenic climate change—A review," *Energy Policy*, vol. 52, pp. 797–809, 2013.

[4] M. Aresta, A. Dibenedetto, and A. Angelini, "The changing paradigm in CO_2 utilization," *Journal of CO_2 Utilization*, vol. 3-4, pp. 65–73, 2013.

[5] M. Liu, Y. Yi, L. Wang, H. Guo, and A. Bogaerts, "Hydrogenation of Carbon Dioxide to Value-Added Chemicals by Heterogeneous Catalysis and Plasma Catalysis," *Catalysts*, vol. 9, no. 3, p. 275, 2019.

[6] H. S. Whang, J. Lim, M. S. Choi, J. Lee, and H. Lee, "Heterogeneous catalysts for catalytic CO_2 conversion into value-added chemicals," *BMC Chemical Engineering*, vol. 1, no. 1, 2019.

[7] S. Roy, A. Cherevotan, and S. C. Peter, "Thermochemical CO_2 Hydrogenation to Single Carbon Products: Scientific and Technological Challenges," *ACS Energy Letters*, vol. 3, no. 8, pp. 1938–1966, Jun. 2018.

[8] V. Arunajatesan, B. Subramaniam, K. Hutchenson, and F. Herkes, "In situ FTIR investigations of reverse water gas shift reaction activity at supercritical conditions," *Chemical Engineering Science*, vol. 62, no. 18-20, pp. 5062–5069, 2007.

[9] C. Kunkel, F. Viñes, and F. Illas, "Transition metal carbides as novel materials for CO_2 capture, storage, and activation," *Energy & Environmental Science*, vol. 9, no. 1, pp. 141–144, 2016.

[10] X. Wang, K. Zhu, Y. Ju, Y. Li, W. Li, J. Xu, and Y. Hou, "Iron carbides: Magic materials with magnetic and catalytic properties," *Journal of Magnetism and Magnetic Materials*, vol. 489, p. 165432, 2019.

[11] S. Li, J. Yang, C. Song, Q. Zhu, D. Xiao, and D. Ma, "Iron Carbides: Control Synthesis and Catalytic Applications in COx Hydrogenation and Electrochemical HER," *Advanced Materials*, p. 1901796, 2019.

[12] S. Bahri, A. M. Venezia, and S. Upadhyayula, "Utilization of greenhouse gas carbon dioxide for cleaner Fischer-Tropsch diesel production," *Journal of Cleaner Production*, vol. 228, pp. 1013–1024, 2019.

[13] M. Racar, F. Faraguna, Z. Glasovac, and A. Jukić, "Experimental modeling and optimization of biodiesel production from waste cooking oil and ethanol using N,N′,N″-tris(3-dimethylaminopropyl)-guanidine as catalyst," *Renewable Energy*, vol. 146, pp. 2374–2379, 2020.

[14] W. Xie and F. Wan, "Guanidine post-functionalized crystalline ZIF-90 frameworks as a promising recyclable catalyst for the production of biodiesel via soybean oil transesterification," *Energy Conversion and Management*, vol. 198, p. 111922, 2019.

[15] N. Pernicone and F. Traina, "Catalyst activation by reduction," *Pure and Applied Chemistry*, vol. 50, no. 9-10, pp. 1169–1191, Jan. 1978.

[16] "Carbon monoxide," Carbon monoxide. [Online]. Available: https://webbook.nist.gov/cgi/cbook.cgi?ID=C630080&Type=IR-SPEC&Index=1. [Accessed: 03-Oct-2019].

[17] "Methane," Methane. [Online]. Available: https://webbook.nist.gov/cgi/cbook.cgi?ID=C74828&Type=IR-SPEC&Index=1. [Accessed: 03-Oct-2019].

[18] C. Binet, M. Daturi, and J.-C. Lavalley, "IR study of polycrystalline ceria properties in oxidised and reduced states," *Catalysis Today*, vol. 50, no. 2, pp. 207–225, 1999.

[19] F. Zhao, Z. Liu, W. Xu, S. Yao, A. Kubacka, A. C. Johnston-Peck, S. D. Senanayake, A.-Q. Zhang, E. A. Stach, M. Fernández-García, and J. A. Rodriguez, "Water-Gas Shift Reaction on Ni–W–Ce Catalysts: Catalytic Activity and Structural Characterization," *The Journal of Physical Chemistry C*, vol. 118, no. 5, pp. 2528–2538, 2014.

[20] C. Li, Y. Sakata, T. Arai, K. Domen, K.-I. Maruya, and T. Onishi, "Carbon monoxide and carbon dioxide adsorption on cerium oxide studied by Fourier-transform infrared spectroscopy. Part 1.—Formation of carbonate species on dehydroxylated CeO2, at room temperature," *Journal of the Chemical Society, Faraday Transactions 1: Physical Chemistry in Condensed Phases*, vol. 85, no. 4, p. 929, 1989.

[21] R. M. Navarro, B. Pawelec, J. M. Trejo, R. Mariscal, and J. G. Fierro, "Hydrogenation of Aromatics on Sulfur-Resistant PtPd Bimetallic Catalysts," *Journal of Catalysis*, vol. 189, no. 1, pp. 184–194, 2000.

[22] H. Yasuda and Y. Yoshimura, "Hydrogenation of tetralin over zeolite-supported Pd-Pt catalysts in the presence of dibenzothiophene," *Catalysis Letters*, vol. 46, no. 1/2, pp. 43–48, 1997.

[23] K. Hayek, R. Kramer, and Z. Paál, "Metal-support boundary sites in catalysis," *Applied Catalysis A: General*, vol. 162, no. 1-2, pp. 1–15, 1997.

[24] A. R. Puigdollers, P. Schlexer, S. Tosoni, and G. Pacchioni, "Increasing Oxide Reducibility: The Role of Metal/Oxide Interfaces in the Formation of Oxygen Vacancies," *ACS Catalysis*, vol. 7, no. 10, pp. 6493–6513, 2017.

[25] S. Y. Moon, B. Naik, C.-H. Jung, K. Qadir, and J. Y. Park, "Tailoring metal–oxide interfaces of oxide-encapsulated Pt/silica hybrid nanocatalysts with enhanced thermal stability," *Catalysis Today*, vol. 265, pp. 245–253, 2016.

[26] W. Li, H. Wang, X. Jiang, J. Zhu, Z. Liu, X. Guo, and C. Song, "A short review of recent advances in CO2 hydrogenation to hydrocarbons over heterogeneous catalysts," *RSC Advances*, vol. 8, no. 14, pp. 7651–7669, 2018.

[27] G. Prieto, "Carbon Dioxide Hydrogenation into Higher Hydrocarbons and Oxygenates: Thermodynamic and Kinetic Bounds and Progress with Heterogeneous and Homogeneous Catalysis," *ChemSusChem*, vol. 10, no. 6, pp. 1056–1070, Jan. 2017.

[28] O. Tursunov, L. Kustov, and A. Kustov, "A Brief Review of Carbon Dioxide Hydrogenation to Methanol Over Copper and Iron Based Catalysts," *Oil & Gas Sciences and Technology – Revue d'IFP Energies nouvelles*, vol. 72, no. 5, p. 30, 2017.